Cavity Control of Excitons in Two-Dimensional Materials

Simone Latini,*[,†,‡,⊥] Enrico Ronca,*[,†,‡,⊥] Umberto De Giovannini,[†,‡,§] Hannes Hübener,[†,‡] and Angel Rubio*[,†,‡,∥]

†Max Planck Institute for the Structure and Dynamics of Matter, Luruper Chaussee 149, 22761 Hamburg, Germany

‡Center for Free-Electron Laser Science and Department of Physics, University of Hamburg, Luruper Chaussee 149, 22761 Hamburg, Germany
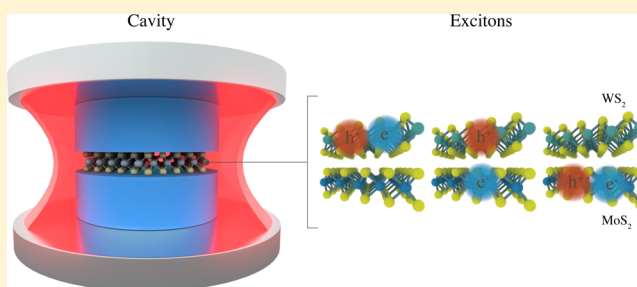
§Dipartimento di Fisica e Chimica, Universitá degli Studi di Palermo, Via Archirafi 36, I-90123, Palermo, Italy

∥Center for Computational Quantum Physics (CCQ), The Flatiron Institute, 162 Fifth Avenue, New York, New York 10010, United States

S *Supporting Information*

ABSTRACT: We propose a robust and efficient way of controlling the optical spectra of two-dimensional materials and van der Waals heterostructures by quantum cavity embedding. The cavity light-matter coupling leads to the formation of exciton−polaritons, a superposition of photons and excitons. Our first-principles study demonstrates a reordering and mixing of bright and dark excitons spectral features and in the case of a type II van-der-Waals heterostructure an inversion of intra- and interlayer excitonic resonances. We further show that the cavity light-matter coupling strongly depends on the dielectric environment and can be controlled by encapsulating the active two-dimensional (2D) crystal in another dielectric material. Our theoretical calculations are based on a newly developed nonperturbative many-body framework to solve the coupled electron−photon Schrödinger equation in a quantum-electrodynamical extension of the Bethe-Salpeter approach. This approach enables the ab initio simulations of exciton−polariton states and their dispersion from weak to strong cavity light-matter coupling regimes. Our method is then extended to treat van der Waals heterostructures and encapsulated 2D materials using a simplified Mott-Wannier description of the excitons that can be applied to very large systems beyond reach for fully ab initio approaches.

KEYWORDS: Exciton−polaritons, quantum cavity, QED, transition metal dichalcogenides, Bethe-Salpeter equation, first-principles

Excitons dominate the optical properties of two-dimensional semiconductors. Single layers of transition metal dichalcogenides (TMDs) have been under intense investigation for their excitonic properties.[1−3] Their weak electronic screening,[4,5] a consequence of the reduced dimensionality, leads to the formation of strongly bound bright and dark excitons which play a fundamental role in a large variety of optoelectronic, spintronic, and valleytronic properties.[6] Furthermore, single layers of TMDs can be stacked in multilayer heterostructures allowing for device engineering with a high degree of freedom.[7−9] Among other designs, bilayers of TMDs with a type II band alignment enables the creation of interlayer excitons, bound electron−hole pairs where the charges are physically confined in two different layers, which show a great potential in photovoltaic applications.[10,11]

Because of their strong coupling to electromagnetic radiation, TMD excitons represent ideal candidates to study strong light-matter coupling in optical cavities.[12−16] In an optical resonator, excitons interact with the quanta of light, generated by the spatial confinement of the cavity, resulting in the formation of new hybrid states with partial matter and partial light character, the "exciton−polaritons".[17−19] These states are inherently different from the bare excitonic states in the material and therefore a variety of novel phenomena can be expected. Envisioned examples comprise new topological phases,[20] light-induced superconductivity,[21] exciton−polariton condensates,[22] and superradiance from exciton insulators.[23]

Here, we present a first-principles theoretical framework, referred to as quantum-electrodynamical Bethe-Salpeter equation (QED-BSE), designed to describe the coupling of excitonic states in crystals embedded in a quantum optical cavity. Our approach goes beyond a simple model Hamiltonian description of exciton polariton by providing a quantitative description of exciton−polariton directly comparable to the experiments. The method requires the exact diagonalization of the exciton-photon equation obtained by extending the widely used many-body Bethe-Salpeter (BSE) formalism[24−27] to QED, under the approximation that the electron−electron interaction is not affected by the photon dressing. This method

represents an alternative to the recently proposed quantum-electrodynamical density functional theory,[17−19,28−33] the latter describing the cavity mediated electron−photon interaction through effective exchange-correlation functionals of the electron and photon densities and currents. Our current method can be used as a starting point to determine such functionals as done in the past for describing the many-body excitonic properties within time-dependent (current) density functional theory.[27] In this work, we demonstrate that by embedding a two-dimensional crystal in a cavity as sketched in Figure 1, excitonic optical activity and energetic ordering can
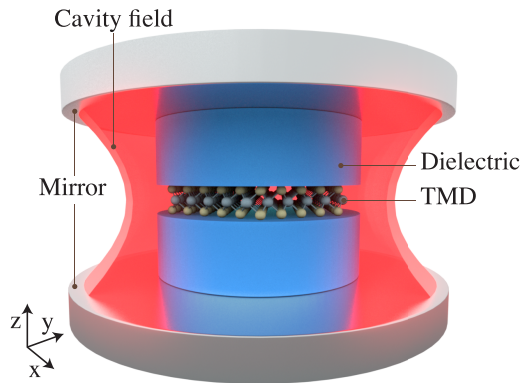

Figure 1. Schematic representation of an encapsulated monolayer TMD in an optical resonator (cavity) including the dielectric media that embeds the 2D material.

be controlled through cavity size, light-matter coupling strength, and encapsulation in a dielectric material. While the reordering of excitonic resonances has been qualitatively demonstrated in the case of molecular systems by means of model Hamiltonians consisting of coupled oscillators for the photonic and excitonic fields,[34,35] here we aim to quantitatively demonstrate similar effects in the context of extended systems.

Within dipolar selection rules there are bright excitons (BE), i.e., accessible as direct transition from the groundstate upon photon absorption, and dark excitons (DE) which are instead not accessible in linear optical spectroscopy.[36] The difficulty to access DE with standard optical spectroscopy poses a challenge for their detection and recent experimental and theoretical works have proposed sophisticated techniques to access them in TMDs.[37,38] Here we address and control the activity of symmetry-forbidden DE through the coupling of the TMD crystal with a quantum cavity which allows direct transitions from the groundstate. More complex types of excitons can be obtained if different monolayers of TMDs with a type II band alignment are stacked together in a van der Waals heterostructure (vdWH).[39] In particular, these type II heterostructures can host excitons where the electron and the hole are localized in different layers, "interlayer excitons", in addition to excitons localized on a single layer, the "intralayer" ones. Here we show how the coupling to an optical cavity can be used to tune the order of the spectral resonances of the different types of excitons, providing a further knob for the design of optical devices based on vdWHs. We also show that the ab initio QED-BSE results can be described by an alternative approach based on the Mott-Wannier model, which we refer to as MW-QED, that represents a computationally inexpensive method able to simplify the QED-BSE approach by simplifying the description

of excitons.[40−42] The MW-QED accurately reproduces the results of the QED-BSE opening the way to the modeling of more complex systems, such as two-dimensional (2D) heterostructures, Moiré patterned twisted bilayer systems, and others, in optical cavities. Finally, we use the MW-QED to characterize the effect produced by a dielectric on the polaritonic spectrum of a single layer of TMD.

Theoretical Framework. The electronic structure of a strongly coupled light-matter system in a cavity requires a nonperturbative treatment of the electron−photon interaction. Fundamentally, light-matter coupling is described by quantum-electrodynamics where the many-body electronic and photonic state is described by a combined Hamiltonian. Specializing this Hamiltonian to the case of a a single cavity mode of frequency Ω and long-wavelength (dipolar) electron−photon coupling, we obtain the first-principles Hamiltonian for perfect loss-less cavity in velocity gauge

$$
\hat{H}_{\text{QED}} = \hat{H}_{\text{el}} + \Omega \hat{a}^\dagger \hat{a} + N_{\text{el}} \frac{A_0^2}{2} (\hat{a}^\dagger + \hat{a})^2
$$
$$
+ A_0 \sum_{ij\mathbf{k}} (\langle \phi_{i\mathbf{k}} | \hat{e}\cdot\hat{p} | \phi_{j\mathbf{k}} \rangle \hat{d}_{i\mathbf{k}}^\dagger \hat{d}_{j\mathbf{k}} \hat{a}^\dagger + h.\,c.\,)
\tag{1}
$$

where $a^\dagger$ and a are the photon creation and annihilation operators respectively, $\hat{H}_{\text{el}}$ is the many-body electronic Hamiltonian, $\hat{d}_{i\mathbf{k}}^\dagger$, $\hat{d}_{j\mathbf{k}}$ are the electronic creation and annihilation operators (with i, j band indices and $\mathbf{k}$ wavevectors in the first Brillouin zone), $\hat{p}$ is the single particle momentum operator, N_{el} is the number of electrons, $\hat{e}$ is the polarization of the photon, and A_0 is the vector potential amplitude. As the coupling of photons to the electronic structure occurs via the creation/annihilation of neutral electron−hole pairs, it is natural to approximate the eigenstates of the many-body electronic Hamiltonian by its excitonic eigenstates, i.e. $\hat{H}_{\text{el}} | \Psi_n^{\text{exc}} \rangle \simeq \epsilon_n^{\text{exc}} | \Psi_n^{\text{exc}} \rangle$. Within this assumption we can accurately describe a regime where the concentration of excitons is low enough to neglect exciton−exciton interaction, which is the case for nonpumped cavities. Under the approximation that the electron−hole Coulomb interaction that binds the exciton is not affected by the photons in the cavity, i.e., the screened Coulomb interaction is not dressed by the cavity photons, the QED Hamiltonian can be expanded in the excitonic basis as follows

$$
\langle \Psi_n^{\text{exc}} | \hat{H}_{\text{QED}} | \Psi_m^{\text{exc}} \rangle = \left[\epsilon_n^{\text{exc}} + \Omega \hat{a}^\dagger \hat{a} + N_{\text{el}} \frac{A_0^2}{2} (\hat{a}^\dagger + \hat{a})^2 \right] \delta_{nm}
$$
$$
+ A_0 (\mathcal{M}_{nm}^{\text{exc}} \hat{a}^\dagger + \mathcal{M}_{mn}^{\text{exc}*} \hat{a})
\tag{2}
$$

where $\mathcal{M}_{nm}^{\text{exc}} = \sum_{ij\mathbf{k}} \langle \phi_{i\mathbf{k}} | \hat{e}\cdot\hat{p} | \phi_{j\mathbf{k}} \rangle \langle \Psi_n^{\text{exc}} | \hat{d}_{i\mathbf{k}}^\dagger \hat{d}_{j\mathbf{k}} | \Psi_m^{\text{exc}} \rangle$ are excitonic matrix elements of the bilinear dipole electron−photon coupling and $\phi_{i\mathbf{k}}$ are single particle Bloch functions. In this framework, the excitonic states can be expressed as a linear combination of singly excited electronic determinants, where the coefficients of the linear combination are given by the solution of the BSE,[25−27] $| \Psi_n^{\text{exc}} \rangle = \sum_{cv\mathbf{k}} A_{cv\mathbf{k}}^n \hat{d}_{c\mathbf{k}}^\dagger \hat{d}_{v\mathbf{k}} | \Psi_0 \rangle$ with $A_{cv\mathbf{k}}^n$ being the BSE coefficients, or envelope functions and c and v indices running over conduction and valence bands, respectively. The electronic groundstate $| \Psi_0 \rangle$ instead is assumed to be a single determinant of only valence states and we define $| \Psi_{n=0}^{\text{exc}} \rangle = | \Psi_0 \rangle$.

In this work, we consider the nondispersive (momentum independent) excitonic states localized around the K-points of the Brillouin zone of the TMD, which are the most relevant for
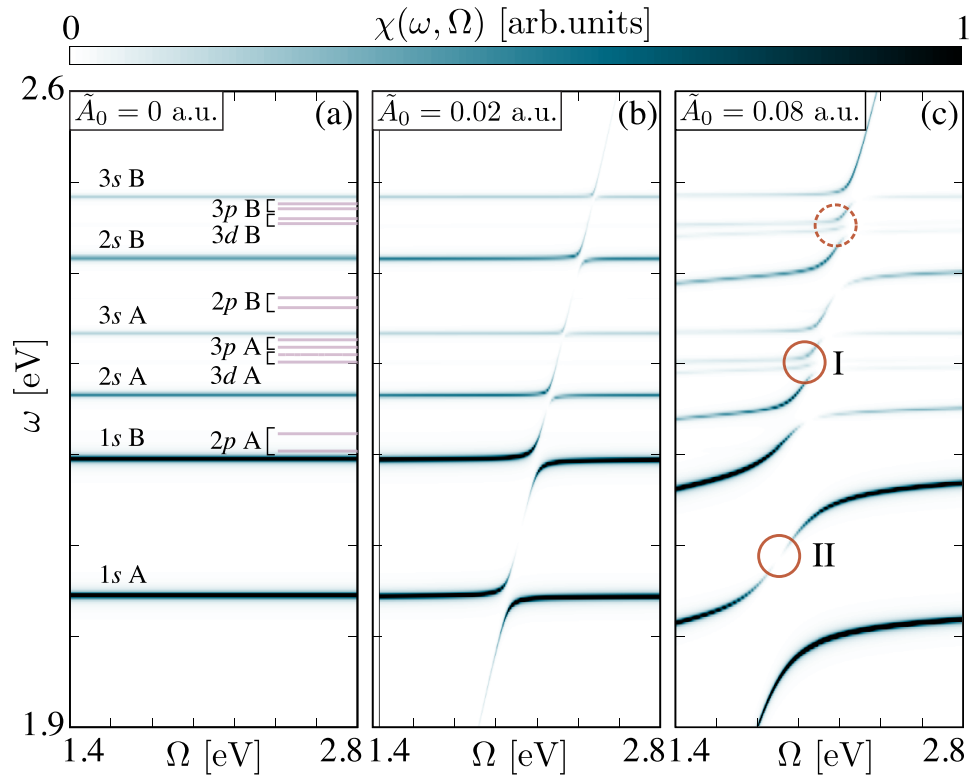
Figure 2. Exciton−polariton spectra of MoS$_2$ in a quantum cavity as a function of cavity mode frequency Ω and for three different coupling strength $\tilde{A}_0$. (a) For no coupling to the cavity mode, the optical spectrum displays a series of spin−orbit split A and B excitons where only excitons with s symmetry appear, i.e., are bright. DE are reported in red segments. (b) For a weaker coupling, excitons hybridize with the cavity photon to form exciton polaritons resulting in Rabi splitting of the bright exciton lines. (c) For the stronger coupling value, the Rabi splitting becomes more pronounced and additional polariton features appear where bright polariton branches cross dark exciton states. The broadening parameter used for all plots is $\eta = 1.4$ meV.

the optoelectronic properties of TMDs. These excitonic states occur in two spin-orthogonal non-hydrogenic series, each of which is accurately described by a spin-independent two-band BSE, where only a single valence and a single conduction band are taken into account.[42] With this simplification, the matrix elements appearing in eq 2 have one of the two following structures

$$\mathcal{M}_{0n}^{exc} = \sum_{\mathbf{k}} A_{\mathbf{k}}^n \langle \phi_{v\mathbf{k}} | \hat{e} \cdot \hat{p} | \phi_{c\mathbf{k}} \rangle \tag{3}$$

$$\mathcal{M}_{nm}^{exc} = N_{el} \sum_{\mathbf{k}} A_{\mathbf{k}}^{m*} A_{\mathbf{k}}^n [\langle \phi_{c\mathbf{k}} | \hat{e} \cdot \hat{p} | \phi_{c\mathbf{k}} \rangle - \langle \phi_{v\mathbf{k}} | \hat{e} \cdot \hat{p} | \phi_{v\mathbf{k}} \rangle] \tag{4}$$

The matrix elements in eq 3 are those that dictate the dark/bright nature of the excitonic states. Those in eq 4, instead, are mixing the character of the excitonic states so that bright to dark or dark to bright transitions can occur.

Below we show first-principles results for MoS$_2$ obtained by first solving the BSE with the GPAW code[43,44] (see Supporting Information for calculation details) and subsequently diagonalizing the QED Hamiltonian of eq 2 in a mixed exciton−photon product state basis $|\Psi_n^{exc}\rangle \otimes |\gamma\rangle$, where $|\gamma\rangle$ are the eigenfunctions of the photonic harmonic oscillator. We then extract energies ($E_I^{pol}(\Omega)$) and corresponding eigenfunctions ($|\Psi_I^{pol}(\Omega)\rangle = \sum_{n\gamma} C_{n\gamma}^I |\Psi_n^{exc}\rangle \otimes |\gamma\rangle$) for the exciton−polariton eigenstates. As for the photonic part, we consider the first nonzero photon mode ($\Omega = \pi c/L_\perp$) with out-of-plane wavevector and in-plane electric field which is able to couple to the MoS$_2$ in-plane excitonic dipole. For our quasi-2D cavity

configuration, the vector potential amplitude A_0 is frequency independent, unlike in the 3D case, indeed $A_0 = 1/\sqrt{SL_\perp\Omega} = 1/\sqrt{2\pi cS}$, where S is the in-plane area of the cavity. Furthermore, we stress that the single mode approximation is valid for polaritons with energies lower than the energy of the second photon mode ($\Omega = 2\pi c/L_\perp$). In the Supporting Information, we show that including higher energy modes does not change the conclusions discussed below. We note that diagonalization of eq 2 is equivalent to solving a CI-singles in the presence of a photon mode. In particular, excited states of the material are expressed as linear combinations of singly excited determinants starting from the ground state and subsequently coupled, through the diagonalization, to the photonic degrees of freedom.

Results. In order to visualize the experimentally measurable exciton−polariton dispersion, we calculate the matter component of the full optical response $\chi(\omega, \Omega)$ applying linear response theory on the polaritonic states[19,33]

$$\chi(\omega, \Omega) = \sum_I \frac{\mathcal{M}_{0I}^{pol} \mathcal{M}_{I0}^{pol}}{\omega - E_I^{pol}(\Omega) + E_0^{pol}(\Omega) + i\eta} \tag{5}$$

where $\mathcal{M}_{IJ}^{pol} = \langle \Psi_I^{pol} | \hat{p} | \Psi_J^{pol} \rangle = \sum_{nm\gamma} C_{n\gamma}^{I*} C_{m\gamma}^J \mathcal{M}_{nm}^{exc}$ and $i\eta$ is a small artificial imaginary broadening. Such a quantity represents the independent particle polarizability of the polariton to a weak external field coupling with the matter component. An equivalent quantity can be also formulated to investigate the photonic counterpart of the polariton.

Comparison between the matter and photon spectral functions is presented in Figure S3 of the Supporting Information.

The formation of exciton−polaritons results in a richer optical response as compared to the bare excitonic response. In Figure 2 we show the cavity polariton spectrum of MoS_2 as a function of mode energy and for different coupling strength $\tilde{A}_0 = A_0/N_{el}$. Here the coupling strength arises from a microscopical definition whereas in practice it can be controlled by the cavity geometry and manufacturing parameters.[45]

Without any electron−photon coupling ($\tilde{A}_0 = 0$), the spectrum features only the bare BEs as shown in Figure 2a, characterized by the common spin−orbit split A and B exciton series (see Supporting Information).[46] Bound excitons in TMDs have atom-like spherical symmetries, following the usual pattern of s, p, d angular momentum quantum numbers and consequently are subject to atomic like selection rules.[37] Only excitons with s-type symmetry are accessible from the ground state through direct absorption of photons. The p and d-type excitons instead can be classified as DEs and are indicated with lines in Figure 2a for reference.

In the weaker coupling regime (c.f. Figure 2b) the formation of an exciton−polariton is accompanied by the characteristic appearance of avoided crossing in the energy dispersion, which results from the hybridization between the linear dispersing photon branch and the nondispersive exciton branches. For a given cavity frequency within the hybridization region, this is detectable as a splitting of the exciton peak into two separate peaks, the Rabi splitting. The formation of lower and upper polariton branches results in a reordering of the energy of bright and dark excitonic resonances which can be of technological relevance for stabilizing long-lived dark excitonic states.

For the stronger coupling (c.f. Figure 2c), the interaction between the cavity photon and the DE results in the appearance of new spectral features marked by circles in the figure. Specifically, we can identify additional splittings (I)/interruptions (II) signature of a cavity-induced optical modulation. It is important to mention that the mixing between bright and dark excitons discussed here is possible only for DE forbidden by symmetry of the wave function.[37] Different kinds of dark excitons like the ones originating from spin-selection rules or beyond dipole selection rules are not discussed in this work.[47] In this stronger coupling regime ($\tilde{A}_0 = 0.08$), we performed calculations also for different TMDs ($MoSe_2$, WS_2, and WSe_2, see Supporting Information) observing qualitatively equivalent features. It is worth noting that for the most bound exciton of WS_2 we obtain a Rabi splitting of ∼22 meV in line with experimental values measured by Flatten et al. (∼20−70 meV).[12] Although it is hard to assess the exact coupling conditions under which the experiment has been performed, this comparison shows that the coupling values used here are on the lower end of the experimentally accessible values. The coupling values used in the results are also in line with the typical sizes of the cavity used in the experiments, which are in the micrometer to nanometer range. In particular, using the $\tilde{A}_0$ definition presented above, a coupling value of ∼0.08 a.u. and an electron density of 0.114 el/Å^2, like in the case of MoS_2, corresponds to a cavity area of about $0.25 \mu m^2$.

Further insight into the structure of these dark polaritons is provided by the analysis shown in Figure 3. The panels quantify the contribution of the different excitonic states to the optically active polariton states at specific cavity energy along
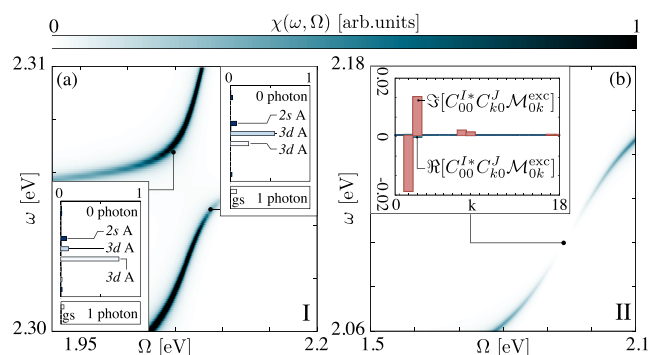

Figure 3. (a) Enlarged view of the dark exciton for the region highlighted in Figure 2 by the circle (I). The insets show the composition of the polariton eigenstates (see text) for points on the lower and upper branch. The compositions are taken as the expansion coefficients of the polaritonic eigenstates in exciton−photon product state basis $|\Psi_n^{exc}\rangle \otimes |\gamma\rangle$. The involved excitonic states are categorized in boxes according to the photon sectors to which they are associated, i.e., $|n\rangle = |0\rangle, |1\rangle$. (b) Enlarged view of a point where the polariton vanished exactly between two consecutive bright exciton lines, highlighted in Figure 2 by the circle (II). The inset shows the real and imaginary parts of the matrix elements contributing to this feature (see text).

the dispersion branches shown in Figure 2. The decomposition of the polariton in Figure 3a, which is a zoom-in of the circle (I) in Figure 2c, shows that it is predominantly the 3d DE that is creating the polaritonic eigenstate. However, it is only because of the photon mediated coupling to the 2s BE that the 3d DE acquires a finite optical cross section. More specifically, the coupling between the two states happens within the $\gamma = 0$ photon sector meaning that there is not an actual absorption or emission of photons in the mixing process but rather both an absorption and subsequent emission (or vice versa) to and from a virtual p-like state in the $\gamma = 1$ photon sector. Because of the hydrogenic-like selection rules, there is no possible excitation/relaxation path between a bright s-like state and dark p-like, i.e., "d"-like states cannot function as virtual states, therefore one does not get a finite oscillator strength. As demonstrated by the insets in Figure 3a, both the lower and upper branch of the DE polariton have a similar composition.

Although Figure 3a illustrates how the cavity coupling reveals hidden (dark) states of a material, we observe another peculiarity in the polariton dispersion in Figure 3b, which corresponds to the circle (II) in Figure 2c. Through the cavity we can induce a quench of the optical activity within the polariton branch connecting two BEs, i.e., the spectral response vanishes completely between two consecutive BE lines. In this case, such a dimming of the polariton branch is not originating from the contribution of DE states but instead is the result of an interesting destructive interference between the optical transition amplitudes from the exciton lines connected by the photon branch. The destructive interference is demonstrated in the inset of Figure 3b which reports the real and imaginary part of the transition amplitude from the groundstate to the 1s A and 1s B excitonic states, the states that make up most of the polariton state.

The QED-BSE method illustrated above requires considerable computational effort and it is therefore limited to few layers of lattice matched (commensurate) TMDs. The polaritonic physics can be well reproduced by replacing the BSE part in the QED-BSE with the Mott-Wannier (MW)
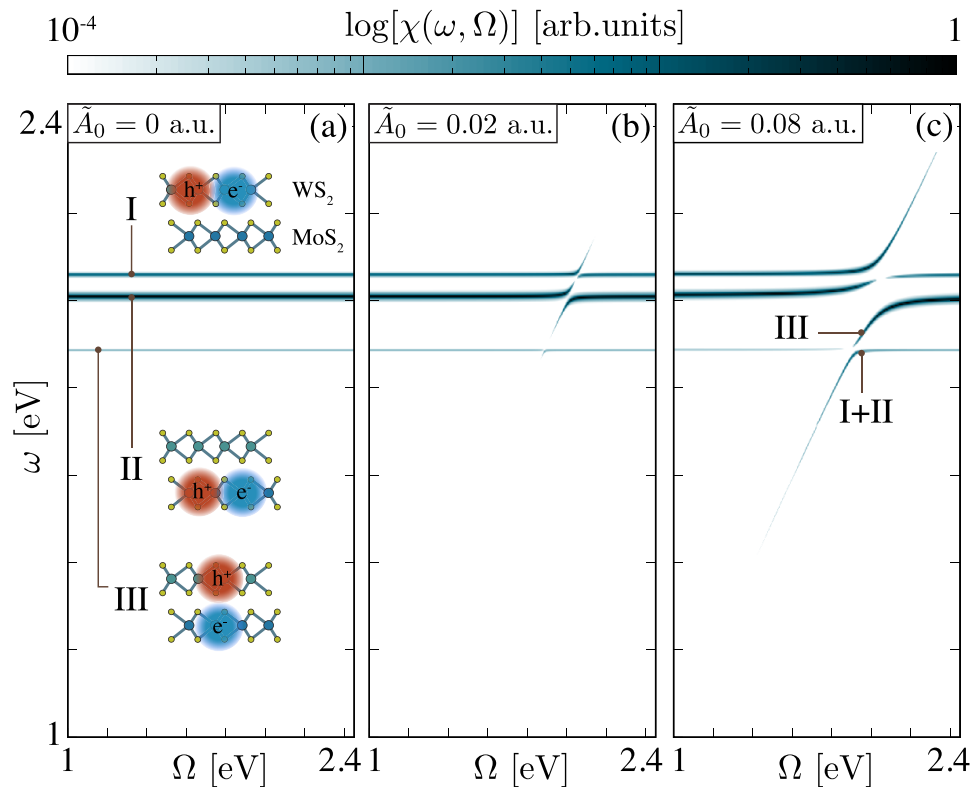
Figure 4. Exciton−polariton spectra of the MoS_2−WS_2 bilayer type-II vdWH as a function of cavity mode frequency Ω and for three different coupling strength $\tilde{A}_0$ in a.u.. Only the lowest bound inter- and intralayer excitons are considered. (a) Without coupling to the cavity mode, the optical spectrum consists of nondispersive optical spectral lines with interlayer exciton lying at lower transition energy than the intralayer exciton ones. (b) For the weaker coupling, both intra and interlayer exciton lines undergo a Rabi splitting, however, due to the lower coupling with the cavity mode, the splitting for the interlayer excitons is much smaller (barely noticeable in the figure) than for the intralayer ones. (c) For the stronger coupling value, the Rabi splitting for the interlayer excitons becomes sizable and the overall spectrum is drastically different from the uncoupled one. We stress that through the cavity mode we are able to invert the order of the intra- and interlayer spectral lines. The broadening parameter used for the plots is η = 1.4 meV.

equation, hence considerably reducing the computational cost and more importantly giving access to exciton−polariton physics in more complex materials such as encapsulated 2D crystals and van der Waals heterostructures. In this approach the bound excitons are described by an hydrogen-like Schrödinger equation that provides the exciton envelope functions and hence allows the evaluation of the exciton−dipole matrix elements $\mathcal{M}_{mn}^{exc}$ of the QED-BSE approach as explained in the Supporting Information.

We apply the MW-QED to calculate the optical response of a vdWH consisting of MoS_2 and WS_2 bilayer. MoS_2 and WS_2 form a type-II heterostructure where the band edges of the two materials are aligned in a staggered fashion and which can host interlayer excitons along with intralayer ones in each of the two layers.[39,48] For this particular bilayer choice, because of quasi-commensurability of the lattice of MoS_2 and WS_2 the QED-BSE has been used to further confirm the validity of the QED-MW presented in the following. However, for more general noncommensurate vdWHs the only feasible approach for simulating exciton−polariton properties is the QED-MW one. The cavity frequency-dependent optical response of such a structure for the most highly bound 1s intra- and interlayer excitons is reported in Figure 4. Including higher lying excitons does not affect the results presented here because the corresponding spectral features would appear in a higher energy window. The use of norm-conserving PAW-setups is needed to obtain the correct energy level alignment. Details on

the method used to calculate the uncoupled excitonic resonances are discussed in the Supporting Information. Figure 4a shows the optical spectrum of the vdWH without coupling with the cavity mode. Here, as indicated by the cartoons, the lower energy nondispersive spectral line represents the optical transitions to the interlayer exciton whereas the higher energy ones are the transition to the intralayer excitons. The oscillator strength of the former is 2 orders of magnitude lower than the one of the intralayer excitons, a direct consequence of the spatial separation of the bound electron−hole pair, justifying the weaker brightness observed in the spectrum. In Figure 4, the coupling with the cavity mode is switched on and the typical polaritonic branches appear with a sizable Rabi splitting for the intralayer and barely noticeable one for the interlayer one. The difference in Rabi splitting is, once again, a consequence of the weak interlayer exciton-light coupling. Similar to the case of monolayer MoS_2 shown in Figure 3b, the interference between the transition to the two intralayer excitons results in a vanishing polariton branch. In the calculations, such an interference arises from the fact that the exciton wave functions of the two intralayer excitons have the same phase. While it is unsure whether this can be directly observed in experiment because any possible mechanism of dephasing would destroy the effect, one could potentially realize the interference by using external lasers to fix the relative phase of the different intralayer excitons. Finally, in the stronger coupling regime, shown in Figure 4c, the optical

response is drastically modified and even the Rabi splitting of the interlayer exciton line is now appreciable. More interestingly, a similar analysis of the polaritonic wave functions as the one discussed for Figure 3c shows that the energetic ordering of the transitions to intra and interlayer excitons is modified, as indicated in the panel. In particular, the lower polariton branch at transition energies lower than the interlayer exciton resonance has now a non-negligible intra-layer exciton composition. We stress that the reordering of the excitonic resonances is possible because of the different light-exciton coupling strength for the different types of excitons. From a practical point of view, the relative light-matter coupling strength for inter- and intralayer excitons can be controlled by (i) building active vdW-bilayers out of monolayers with different thicknesses and dielectric properties and (ii) choosing a different embedding material to change the dielectric environment of the cavity. For example, a higher coupling strength for the interlayer excitons can be achieved in a vdW-bilayer made of crystals with a lower thickness and lower dielectric screening, whereas a lower coupling strength can be obtained choosing an embedding material with a higher dielectric function. These calculations show the potential of cavity engineering for the optical design of functional devices where either intralayer or interlayer excitons can be excited on demand.

The MW-QED also provides a computationally inexpensive way of assessing the effect of embedding an active 2D materials in a bulk dielectric[42] (as sketched in Figure 1). The effect of the dielectric environment is accounted for in the MW description through its bulk dielectric constant κ, c.f. refs 42 and 49 and Supporting Information for a detailed description of the method. The effect of environmental screening is three-fold: (i) extra-screening of the electron−hole Coulomb interaction, (ii) renormalization of photon dispersion $(\omega = \omega_c/\sqrt{(\kappa)})$ which now propagates in dielectric medium, and (iii) renormalization of the effective vector potential amplitude of the cavity $\overline{A}_0(\kappa) = \tilde{A}_0/\kappa$.[40]

In Figure 5a, we show the polariton dispersion of MoS_2 for fixed coupling strength $\tilde{A}_0$ and for various values of dielectric constants κ for the substrate material. The most striking feature is the change in the slope of the photon line due to the propagation in the cavity dielectric. This shifts the position of the polariton resonances. Furthermore, due to the change of the screened Coulomb interaction, the higher lying excitons are squeezed in energy toward the first excitonic state (c.f. Supporting Information). Figure 5c shows the dependence of the Rabi-splitting of the first three BEs (1s, 2s, 3s of the A series) as a function of the dielectric constant of the encapsulating material. We compare the splitting of the calculated dispersion with the Rabi splitting of the corresponding Jaynes-Cummings model where only two levels at a time (the groundstate and one of the excitons) are taken into account. Notably, only for small dielectric constants there are deviations from Jaynes-Cummings splitting indicating that for larger effective couplings $\overline{A}_0$ the two level approximation breaks down.

Conclusion. The QED-BSE formalism we presented here is a first-principles approach to the properties of polaritons in optical cavities. We demonstrate how it gives rise to complex polaritons dispersions, where hybridizations of polaritons manifest in features originating from DE. We also show how polaritonic interference could result in transparency and could
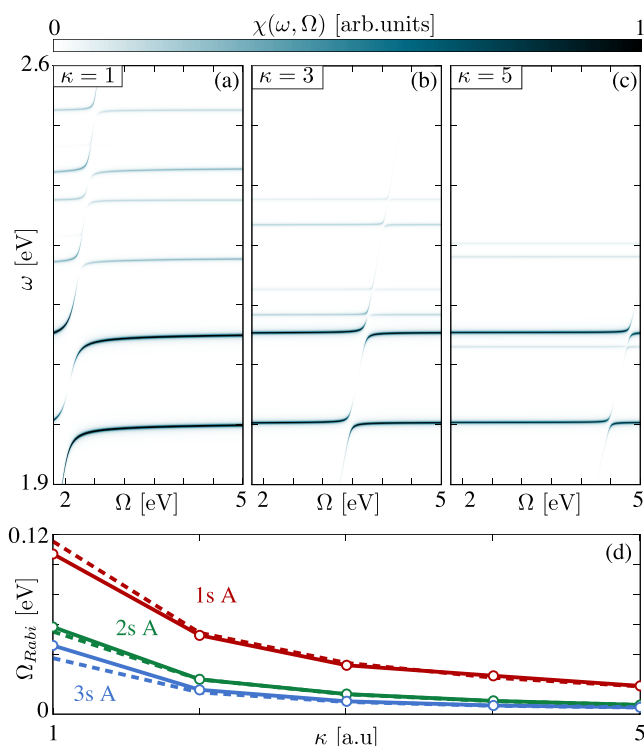

Figure 5. Polariton dispersion of MoS_2 for different values of dielectric constant κ of the substrate (a−c), calculated with the MW model and with $\tilde{A}_0 = 0.05$ a.u. Dependence of the Rabi splitting of the 1s A, 2s A and 3s A states on the dielectric constant (d). Solid lines with circles are the Rabi splitting calculated with the MW model, dashed lines are calculated from the Jaynes-Cummings model as $\Omega_{\text{Rabi}} = 2A_0 \mathcal{M}_{0n}^{\text{exc}}$.

be possibly achieved through laser control. We illustrate how the Mott-Wannier model for bound excitons can be used to obtain the relevant dipole matrix elements that enter the QED equations and thus provide a readily applicable method to compute such polariton properties. This method can be extended to account for the dielectric screening of materials inside the cavity which gives access to a large variety of van der Waals layered systems. In particular, in the case of a type II vdWH we demonstrate the possibility of engineering cavity-matter coupling and change the relative energy ordering of intra- and interlayer excitons. The QED-BSE and QED-MW model presented here are the first ab initio methods aimed at the design, understanding, and control of the optoelectronic properties of materials embedded in quantum cavities.

■ ASSOCIATED CONTENT

ⓢ Supporting Information

The Supporting Information is available free of charge on the ACS Publications website at DOI: 10.1021/acs.nanolett.9b00183.

extensive computational details, convergence tests with respect to the number of excitonic states, number of photons and number of cavity modes included in the calculation, details about the Mott-Wannier methodology, and a comparison between the matter and photon spectral functions (PDF)

■ AUTHOR INFORMATION

Corresponding Authors
*E-mail: simone.latini@mpsd.mpg.de.
*E-mail: enrico.ronca@mpsd.mpg.de.
*E-mail: angel.rubio@mpsd.mpg.de.

ORCID
Simone Latini: 0000-0001-9553-5259
Enrico Ronca: 0000-0003-0494-5506
Umberto De Giovannini: 0000-0002-4899-1304
Hannes Hübener: 0000-0003-0105-1427

Author Contributions
[⊥]S.L. and E.R. contributed equally to this work.

Notes
The authors declare no competing financial interest.

■ REFERENCES

(1) Manzeli, S.; Ovchinnikov, D.; Pasquier, D.; Yazyev, O. V.; Kis, A. *Nat. Rev. Mater.* **2017**, *2*, 17033.

(2) Wang, G.; Chernikov, A.; Glazov, M. M.; Heinz, T. F.; Marie, X.; Amand, T.; Urbaszek, B. *Rev. Mod. Phys.* **2018**, *90*, 021001.

(3) Ugeda, M. M.; Bradley, A. J.; Shi, S.-F.; da Jornada, F. H.; Zhang, Y.; Qiu, D. Y.; Ruan, W.; Mo, S.-K.; Hussain, Z.; Shen, Z.-X.; et al. *Nat. Mater.* **2014**, *13*, 1091.

(4) Ramasubramaniam, A. *Phys. Rev. B: Condens. Matter Mater. Phys.* **2012**, *86*, 115409.

(5) Cudazzo, P.; Tokatly, I. V.; Rubio, A. *Phys. Rev. B: Condens. Matter Mater. Phys.* **2011**, *84*, 085406.

(6) Schaibley, J. R.; Yu, H.; Clark, G.; Rivera, P.; Ross, J. S.; Seyler, K. L.; Yao, W.; Xu, X. *Nat. Rev. Mater.* **2016**, *1*, 16055.

(7) Kim, J.; Jin, C.; Chen, B.; Cai, H.; Zhao, T.; Lee, P.; Kahn, S.; Watanabe, K.; Taniguchi, T.; Tongay, S. *Science Adv.* **2017**, *3*, e1700518.

(8) Gao, G.; Gao, W.; Cannuccia, E.; Taha-Tijerina, J.; Balicas, L.; Mathkar, A.; Narayanan, T. N.; Liu, Z.; Gupta, B. K.; Peng, J.; et al. *Nano Lett.* **2012**, *12*, 3518−3525.

(9) Geim, A. K.; Grigorieva, I. V. *Nature* **2013**, *499*, 419.

(10) Hong, X.; Kim, J.; Shi, S.-F.; Zhang, Y.; Jin, C.; Sun, Y.; Tongay, S.; Wu, J.; Zhang, Y.; Wang, F. *Nat. Nanotechnol.* **2014**, *9*, 682.

(11) Jin, C.; Ma, E. Y.; Karni, O.; Regan, E. C.; Wang, F.; Heinz, T. F. *Nat. Nanotechnol.* **2018**, *13*, 994.

(12) Flatten, L. C.; He, Z.; Coles, D. M.; Trichet, A. A. P.; Powell, A. W.; Taylor, R. A.; Warner, J. H.; Smith, J. M. *Sci. Rep.* **2016**, *6*, 33134.

(13) Chervy, T.; Azzini, S.; Lorchat, E.; Wang, S.; Gorodetski, Y.; Hutchison, J. A.; Berciaud, S.; Ebbesen, T. W.; Genet, C. *ACS Photonics* **2018**, *5*, 1281−1287.

(14) Slootsky, M.; Liu, X.; Menon, V. M.; Forrest, S. R. *Phys. Rev. Lett.* **2014**, *112*, 076401.

(15) Liu, X.; Galfsky, T.; Sun, Z.; Xia, F.; Lin, E.-c.; Lee, Y.-H.; Kéna-Cohen, S.; Menon, V. M. *Nat. Photonics* **2015**, *9*, 30.

(16) Sun, Z.; Gu, J.; Ghazaryan, A.; Shotan, Z.; Considine, C. R.; Dollar, M.; Chakraborty, B.; Liu, X.; Ghaemi, P.; Kéna-Cohen, S.; et al. *Nat. Photonics* **2017**, *11*, 491.

(17) Flick, J.; Ruggenthaler, M.; Appel, H.; Rubio, A. *Proc. Natl. Acad. Sci. U. S. A.* **2017**, *114*, 3026.

(18) Flick, J.; Schafer, C.; Ruggenthaler, M.; Appel, H.; Rubio, A. *ACS Photonics* **2018**, *5*, 992−1005.

(19) Ruggenthaler, M.; Tancogne-Dejean, N.; Flick, J.; Appel, H.; Rubio, A. *Nat. Rev. Chem.* **2018**, *2*, 0118.

(20) Sheikhan, A.; Brennecke, F.; Kollath, C. *Phys. Rev. A: At., Mol., Opt. Phys.* **2016**, *94*, 061603.

(21) Sentef, M. A.; Ruggenthaler, M.; Rubio, A. *Science Advances* **2018**, *4*, No. eaau6969.

(22) Byrnes, T.; Kim, N. Y.; Yamamoto, Y. *Nat. Phys.* **2014**, *10*, 803.

(23) Mazza, G.; Georges, A. *Phys. Rev. Lett.* **2019**, *122*, 017401.

(24) Salpeter, E. E.; Bethe, H. A. *Phys. Rev.* **1951**, *84*, 1232−1242.

(25) Rohlfing, M.; Louie, S. G. *Phys. Rev. Lett.* **1998**, *81*, 2312−2315.

(26) Rohlfing, M.; Louie, S. G. *Phys. Rev. B: Condens. Matter Mater. Phys.* **2000**, *62*, 4927−4944.

(27) Onida, G.; Reining, L.; Rubio, A. *Rev. Mod. Phys.* **2002**, *74*, 601−659.

(28) Tokatly, I. V. *Phys. Rev. Lett.* **2013**, *110*, 233001.

(29) Ruggenthaler, M.; Flick, J.; Pellegrini, C.; Appel, H.; Tokatly, I. V.; Rubio, A. *Phys. Rev. A: At., Mol., Opt. Phys.* **2014**, *90*, 012508.

(30) Pellegrini, C.; Flick, J.; Tokatly, I. V.; Appel, H.; Rubio, A. *Phys. Rev. Lett.* **2015**, *115*, 093001.

(31) Flick, J.; Ruggenthaler, M.; Appel, H.; Rubio, A. *Proc. Natl. Acad. Sci. U. S. A.* **2015**, *112*, 15285−15290.

(32) Rokaj, V.; Welakuh, D. M.; Ruggenthaler, M.; Rubio, A. *J. Phys. B: At., Mol. Opt. Phys.* **2018**, *51*, 034005.

(33) Flick, J.; Welakuh, D. M.; Ruggenthaler, M.; Appel, H.; Rubio, A. **2018**, arXiv:1803.02519. arXiv.org e-Print archive. https://arxiv.org/abs/1803.02519.

(34) Du, M.; Martnez-Martinez, L. A.; Ribeiro, R. F.; Hu, Z.; Menon, V. M.; Yuen-Zhou, J. *Chem. Sci.* **2018**, *9*, 6659−6669.

(35) Polak, D.; Jayaprakash, R.; Leventis, A.; Fallon, K. J.; Coulthard, H.; Petty, I., Anthony, J.; Anthony, J.; Bronstein, H.; Lidzey, D. G.; Clark, J. et al. arXiv e-prints **2018**, arXiv:1806.09990.28

(36) Cao, T.; Wu, M.; Louie, S. G. *Phys. Rev. Lett.* **2018**, *120*, 087402.

(37) Ye, Z.; Cao, T.; O'Brien, K.; Zhu, H.; Yin, X.; Wang, Y.; Louie, S. G.; Zhang, X. *Nature* **2014**, *513*, 214−218.

(38) Loh, K. P. *Nat. Nanotechnol.* **2017**, *12*, 837−838.

(39) Latini, S.; Winther, K. T.; Olsen, T.; Thygesen, K. S. *Nano Lett.* **2017**, *17*, 938−945.

(40) Grosso, G.; Parravicini, G. *Solid State Physics*; Elsevier Science, 2000.

(41) Keldysh, L. V. *JETP Lett.* **1979**, *29*, 658.

(42) Latini, S.; Olsen, T.; Thygesen, K. S. *Phys. Rev. B: Condens. Matter Mater. Phys.* **2015**, *92*, 245123.

(43) Mortensen, J. J.; Hansen, L. B.; Jacobsen, K. W. *Phys. Rev. B: Condens. Matter Mater. Phys.* **2005**, *71*, 035109.

(44) Enkovaara, J.; Rostgaard, C.; Mortensen, J. J.; Chen, J.; Dułak, M.; Ferrighi, L.; Gavnholt, J.; Glinsvad, C.; Haikola, V.; Hansen, H. A.; et al. *J. Phys.: Condens. Matter* **2010**, *22*, 253202.

(45) Flick, J.; Rivera, N.; Narang, P. *Nanophotonics* **2018**, *7*, 1479−1501.

(46) Qiu, D. Y.; da Jornada, F. H.; Louie, S. G. *Phys. Rev. Lett.* **2013**, *111*, 216805.

(47) Malic, E.; Selig, M.; Feierabend, M.; Brem, S.; Christiansen, D.; Wendler, F.; Knorr, A.; Berghäuser, G. *Phys. Rev. Materials* **2018**, *2*, 014002.

(48) Palummo, M.; Bernardi, M.; Grossman, J. C. *Nano Lett.* **2015**, *15*, 2794−2800.

(49) Andersen, K.; Latini, S.; Thygesen, K. S. *Nano Lett.* **2015**, *15*, 4616−4621.